DC RESISTIVITY MODELLING AND SENSITIVITY ANALYSIS IN ANISOTROPIC MEDIA

by

Mark S. Greenhalgh

B.Sc.

Department of Physics

The University of Adelaide

SA 5005, Australia

Submitted in fulfilment of the requirements for

the degree of Doctor of Philosophy

August 2008

Chapter 6

Fréchet Derivatives in Resistivity Anisotropic Inversion

6.1 Sensitivity Functions

The inversion of electrical resistivity data to reconstruct the conductivity distribution of the subsurface requires knowledge of the Fréchet derivatives, which form the elements of Jacobian matrix of the objective function (Menke, 1989; Lesur *et al.*, 1999). These derivatives give the perturbation in the field quantity (i.e., electric potential or apparent resistivity) for a given perturbation in the medium properties (i.e., conductivity). They vary spatially throughout the medium and need to be computed at each subsurface point for each electrode configuration. The Fréchet derivatives depend not only upon the conductivity but also on the survey geometry (i.e., electrode positions). The derivatives may be viewed as sensitivity functions of the data, and used to indicate the sensitivity variations with various surveying configurations. Thus they are extremely important in optimising experimental design and understanding resolution (Stummer *et al.*, 2004; Maurer and Friedel, 2006).

There are various ways to compute the Fréchet derivatives in resistivity imaging. McGillivray and Oldenburg (1990) made a comparative theoretical study of several methods. Park and Van (1991) derived an implicit expression for the Fréchet derivative in the 3-D problem. Smith and Vozoff (1984) and Sasaki (1994) calculated the Fréchet derivative by solving the differential equations of the finite difference or finite element system. Loke and Barker (1995, 1996) computed the Fréchet derivatives with a homogeneous half space starting model and Broyden's (1965) updating procedure. Spitzer (1998) describes four different methods and presented plots of the sensitivity patterns for homogeneous and simple inhomogeneous models, using common surface and crosshole electrode configurations (pole-pole, pole-dipole etc.). Zhou and Greenhalgh (1999) showed that the most direct and effective way to compute the Fréchet derivatives is in terms of the Green's functions. They developed explicit expressions and a numerical calculation scheme for the Fréchet and second derivatives for a heterogeneous, *isotropic* earth using a finite element approach. Their 2.5-D and 3-D formulations were given for the electric potential as well as for the apparent resistivity, using any electrode array. It is only recently that accurate and efficient computational schemes have been developed for calculating the Green's functions in an anisotropic and inhomogeneous earth (Li and Spitzer, 2005; Zhou *et al.*, 2008)

In this chapter, the earlier analysis is extended to the case of a general *anisotropic*, inhomogeneous medium. To the best of my knowledge such expressions have not been given before.

6.2 Perturbation Analysis

From chapter 2, the Helmholtz equation representing the DC resistivity problem in both 2.5-D and 3-D can be expressed as:

$$D(\boldsymbol{\sigma})G_s = -\frac{1}{c}\delta(r-r_s),$$

(6.1)

where $G_s = \bar{G}_s(r)$ or $G_s = G_s(r)$ for the 2.5-D or 3-D case respectively, for which $c = 2$ or $c = 1$ respectively. The tilde above G denotes spatial Fourier transform with respect to the strike or y direction. The differential operator is defined by

$$D(\boldsymbol{\sigma})G_s = \begin{cases} \vec{\nabla}\cdot\left(\boldsymbol{\sigma}\vec{\nabla}\bar{G}_s\right)-k_y^2\sigma_{yy}\bar{G}_s & r\in\Omega(x,z) \\ \vec{\nabla}\cdot\left(\boldsymbol{\sigma}\vec{\nabla}G_s\right) & r\in\Omega(x,y,z) \end{cases}$$

(6.2)

From this definition one can easily show the operator $D(\sigma)$ is linear,

$$D(\boldsymbol{\sigma}_A + \lambda\boldsymbol{\sigma}_B) = D(\boldsymbol{\sigma}_A) + \lambda D(\boldsymbol{\sigma}_B), \qquad \forall\lambda\in R$$

(6.3)

and self-adjoint for the integration:

$$\int_\Omega W(r)D(\boldsymbol{\sigma})G_s(r)d\Omega = \int_\Omega G_s(r)D(\boldsymbol{\sigma})W(r)d\Omega, \qquad \forall W(r)\in C^1(\Omega)$$

(6.4)

For any small perturbation $\delta\sigma$ in the medium properties, we have

$$D(\boldsymbol{\sigma}+\delta\boldsymbol{\sigma})(G_s + \delta G_s) = -\frac{1}{c}\delta(r-r_s).$$

(6.5)

Applying the linear property and equation (6.1), one obtains

$$D(\boldsymbol{\sigma})\delta G_s = -D(\delta\boldsymbol{\sigma})G_s - D(\delta\boldsymbol{\sigma})\delta G_s. \tag{6.6}$$

To solve the above equation, we employ the conjugate Green's function by placing an adjoint source at the receiver (potential electrode) position and defined by

$$D(\boldsymbol{\sigma})G_p = -\frac{1}{c}\delta(r - r_p), \qquad r, r_p \in \Omega. \tag{6.7}$$

Multiplying δG_s to the above and calculating the integration over the domain in terms of equation (6.4), we have

$$
\begin{aligned}
\delta G_s(r_p) &= -c\int_\Omega G_p(r)D(\boldsymbol{\sigma})\delta G_s(r)d\Omega \\
&= c\int_\Omega G_p(r)D(\delta\boldsymbol{\sigma})G_s(r)d\Omega + o\left(\|\delta\boldsymbol{\sigma}\|^2\right)
\end{aligned}
\tag{6.8}
$$

Substituting equation (6.2) for (6.8), integrating by parts and ignoring the higher order terms, we obtain the linear relationship between the change (perturbation) of the Green's function and the perturbation in the medium properties $\delta\sigma$,

$$
\begin{aligned}
\delta\bar{G}_s(r_p) &= -2\int_\Omega\left[\delta\boldsymbol{\sigma}\vec{\nabla}\bar{G}_s(r)\cdot\vec{\nabla}\bar{G}_p(r) + k_y^2\delta\sigma_{yy}\bar{G}_s(r)\bar{G}_p(r)\right]d\Omega \\
&= -2\int_\Omega\left[\delta\sigma_{xx}\frac{\partial\bar{G}_s}{\partial x}\frac{\partial\bar{G}_p}{\partial x} + \delta\sigma_{xz}\left(\frac{\partial\bar{G}_s}{\partial z}\frac{\partial\bar{G}_p}{\partial x} + \frac{\partial\bar{G}_s}{\partial x}\frac{\partial\bar{G}_p}{\partial z}\right)\right. \\
&\qquad\left. +\delta\sigma_{zz}\frac{\partial\bar{G}_s}{\partial z}\frac{\partial\bar{G}_p}{\partial z} + k_y^2\delta\sigma_{yy}\bar{G}_s(r)\bar{G}_p(r)\right]d\Omega
\end{aligned}
\tag{6.9}
$$

for the 2.5-D case , and

$$
\begin{aligned}
\delta G_s(r_p) &= -\int_\Omega\left[\delta\boldsymbol{\sigma}\vec{\nabla}\bar{G}_s(r)\cdot\vec{\nabla}\bar{G}_p(r)\right]d\Omega \\
&= \int_\Omega\left[\delta\sigma_{xx}\frac{\partial G_s}{\partial x}\frac{\partial G_p}{\partial x} + \delta\sigma_{xy}\left(\frac{\partial G_s}{\partial y}\frac{\partial G_p}{\partial x} + \frac{\partial G_s}{\partial x}\frac{\partial G_p}{\partial y}\right)\right. \\
&\qquad +\delta\sigma_{xy}\left(\frac{\partial G_s}{\partial z}\frac{\partial G_p}{\partial x} + \frac{\partial G_s}{\partial x}\frac{\partial G_p}{\partial z}\right) + \delta\sigma_{yy}\frac{\partial G_s}{\partial y}\frac{\partial G_p}{\partial y} \\
&\qquad\left. +\delta\sigma_{yz}\left(\frac{\partial G_s}{\partial z}\frac{\partial G_p}{\partial y} + \frac{\partial G_s}{\partial y}\frac{\partial G_p}{\partial z}\right) + \delta\sigma_{zz}\frac{\partial G_s}{\partial z}\frac{\partial G_p}{\partial z}\right]d\Omega
\end{aligned}
\tag{6.10}
$$

for the 3-D situation. Here, we have made the assumption that at the boundary of Ω no perturbation occurs in the conductivity $(\delta\boldsymbol{\sigma} = 0)$.

6.3 Fréchet Derivatives

According to equations (6.9) and (6.10) and by applying a model discretisation scheme: either constant-point: $\delta\boldsymbol{\sigma}(r) = \delta\boldsymbol{\sigma}_k \delta(r - r_k)$, $r \in \Omega_k$, or constant block: $\delta\boldsymbol{\sigma}(r) = \delta\boldsymbol{\sigma}_k$, $r \in \Omega_k$, where Ω_k are small sub-domains composing Ω, we obtain the following results for the Fréchet derivatives:

Constant Point Approximation

2.5-D:

$$\frac{\partial G_s(r_p)}{\partial(\sigma_{\alpha\beta})_k} = -\begin{cases} 2F_c^{-1}\left[k_y^2 \overline{G}_s(r_k)\overline{G}_p(r_k)\right], & (\alpha = \beta = y) \\ c_{\alpha\beta}F_c^{-1}\left[\left(\frac{\partial \overline{G}_s}{\partial \alpha}\frac{\partial \overline{G}_p}{\partial \beta} + \frac{\partial \overline{G}_p}{\partial \alpha}\frac{\partial \overline{G}_s}{\partial \beta}\right)_{r_s}\right] & (\alpha, \beta = x, z) \end{cases} \tag{6.11}$$

3-D:

$$\frac{\partial G_s}{\partial(\sigma_{\alpha\beta})_k} = -c_{\alpha\beta}\left(\frac{\partial G_s}{\partial \alpha}\frac{\partial G_p}{\partial \beta} + \frac{\partial G_p}{\partial \alpha}\frac{\partial G_s}{\partial \beta}\right)_{r_s}, \quad (\alpha, \beta = x, y, z) \tag{6.12}$$

or the alternative

Constant Block Approximation

2.5-D:

$$\frac{\partial G_s(r_p)}{\partial(\sigma_{\alpha\beta})_k} = -\begin{cases} 2w_l F_c^{-1}\left[k_y^2\left(\overline{G}_s\overline{G}_p\right)_{r_l}\right], & (\alpha = \beta = y, \quad r_l \in \Omega_k) \\ c_{\alpha\beta}F_c^{-1}\left[\left(\frac{\partial \overline{G}_s}{\partial \alpha}\frac{\partial \overline{G}_p}{\partial \beta} + \frac{\partial \overline{G}_p}{\partial \alpha}\frac{\partial \overline{G}_s}{\partial \beta}\right)_{r_s}\right] & (\alpha, \beta = x, z, \quad r_l \in \Omega_k) \end{cases} \tag{6.13}$$

3-D:

$$\frac{\partial G_s(r_p)}{\partial(\sigma_{\alpha\beta})_k} = -c_{\alpha\beta}w_l\left(\frac{\partial G_s}{\partial \alpha}\frac{\partial G_p}{\partial \beta} + \frac{\partial G_p}{\partial \alpha}\frac{\partial G_s}{\partial \beta}\right)_{r_l} \quad (\alpha, \beta = x, y, z, \quad r_l \in \Omega_k) \tag{6.14}$$

The notation is: $c_{\alpha\beta} = 1$ as $\alpha = \beta$ and $c_{\alpha\beta} = 2$ if $\alpha \neq \beta$. The symbol F_c^{-1} denotes inverse Fourier cosine transformation with respect to wavenumber k_y. The quantity w_l is the product of the Gaussian weights in the various co-ordinate directions involved in a Gaussian quadrature approach to performing the volume integration. The derivative formulae (6.11) – (6.14) may be directly employed for anisotropic resistivity inversion to update the parameter estimates, once the source and adjoint Green's functions have been calculated for each subsurface point. The actual process of computing the Fréchet derivatives is illustrated schematically in figure (6.1).
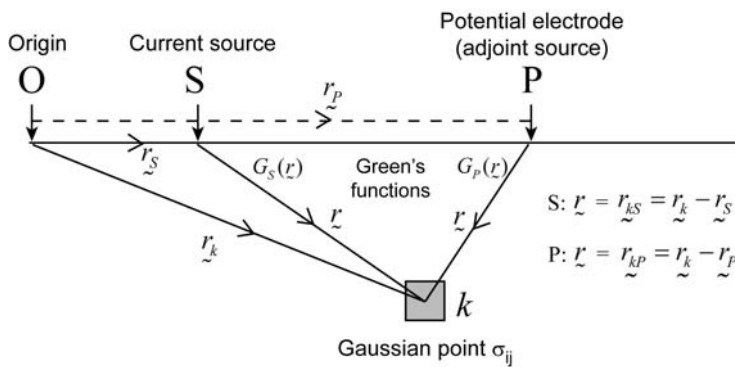
Figure 6.1 Schematic illustration of Frechet derivatives (or sensitivities) at subsurface point k for a true current source at point S and an adjoint source at potential electrode position P. The Green's functions from both sources, and/or their gradients, are required in the formulation

For each subsurface point k we can calculate the sensitivities for a given electrode configuration (source S and receiver P) in terms of the two Green's functions $G_s\left(\vec{r}_{ks}\right)$ and $G_p\left(\vec{r}_{kp}\right)$. For the common four-electrode systems the sensitivities can be computed from the pole-pole responses given above by simple superposition (algebraic addition). Note that summation is implied in the above equations through repetition of the subscripts α and β.

6.4 Numerical Method

Applying a numerical method, such as the finite element method (Li and Spitzer, 2005) or the Gaussian Quadrature Grid method of chapter 4 to the governing equation, one has the following linear equation system:

$$M\left(\boldsymbol{\sigma}\right)\vec{G}_s = \vec{b}_s \tag{6.15}$$

where $\vec{G}_s = \{G_{si}, i = 1, 2, \ldots, N\}$ is the vector whose components are the values of the Green's function at all nodes, $\vec{b}_s = \{\delta_{is}, i = 1, 2, \ldots, N\}$ is the source vector whose components are zero except for the one $(\delta_{ss} = 1)$ at the node coinciding with the source location, and $M(\sigma)$ is a $N \times N$ symmetric matrix, which is calculated by

$$M_{ij}(\boldsymbol{\sigma}) = \begin{cases} 2\int_{\Omega_k} \left[\boldsymbol{\sigma}\vec{\nabla}l_i(r) \cdot \vec{\nabla}l_j(r) + k_y^2 \sigma_{yy} l_i(r) l_j(r) \right] d\Omega & r \in \Omega_k(x, z) \\ \int_{\Omega_k} \left[\boldsymbol{\sigma}\vec{\nabla}l_i(r) \cdot \vec{\nabla}l_j(r) \right] d\Omega & r \in \Omega_k(x, y, z) \end{cases} \tag{6.16}$$

in terms of the Variational Principle and sub-domain or element integration. Here, $l_i(r)$ are the Lagrange interpolants or shape functions. Differentiating equation (6.15) with respect to $(\sigma_{\alpha\beta})_k$, we have

$$M(\boldsymbol{\sigma}) \frac{\partial G_s}{\partial(\sigma_{\alpha\beta})_k} = -\frac{\partial M(\boldsymbol{\sigma})}{\partial(\sigma_{\alpha\beta})_k} G_s. \tag{6.17}$$

In order to solve the above equation, we applied equation (6.15) to multiple source vectors $\vec{I}_n = \left(\vec{b}_{s1}, \vec{b}_{s2}, \ldots, \vec{b}_{sN}\right)$ and corresponding Green's function matrix $\vec{G}_{N \times N} = \left(\vec{G}_{s1}, \vec{G}_{s2}, \ldots, \vec{G}_{sN}\right)$. We have the identity

$$M(\boldsymbol{\sigma}) = \vec{G}_{N \times N} = \vec{I} \tag{6.18}$$

Multiplying the vector $\vec{b}_p^T \vec{G}_{N \times N}^T = \vec{G}_p^T$ to equation (6.16) and applying the symmetry property of $M(\boldsymbol{\sigma})$ and equation (6.18), one obtains the derivatives

$$\frac{\vec{\partial}G_s(r_p)}{\vec{\partial}(\sigma_{\alpha\beta})_k} = -\vec{G}_p^T \frac{\vec{\partial}M(\boldsymbol{\sigma})}{\vec{\partial}(\sigma_{\alpha\beta})_k} \vec{G}_s \tag{6.19}$$

Substituting equation (6.16) for (6.19) and noting that most components of the matrix $\vec{\partial}M(\boldsymbol{\sigma})\big/\vec{\partial}(\sigma_{\alpha\beta})_k$ are zero except for the kth sub-domain Ω_k that has conductivity tensor σ_k, equation (6.19) becomes, for the 2.5-D and 3-D cases respectively,

$$
\begin{aligned}
\frac{\partial G_s(r_p)}{\partial(\sigma_{\alpha\beta})_k} &= -F_c^{-1}\Bigg\{ 2\int_{\Omega_k}\Bigg[\frac{\vec{\partial}\sigma_k}{\vec{\partial}(\sigma_{\alpha\beta})_k}\cdot\vec{\nabla}\Bigg[\sum_i l_i(r)\bar{G}_{pi}\Bigg]\cdot\vec{\nabla}\Bigg[\sum_j l_j(r)\bar{G}_{sj}\Bigg] \\
&\qquad + \frac{\partial\sigma_{yy}}{\partial(\sigma_{\alpha\beta})_k}\Bigg[\sum_i l_i(r)\bar{G}_{pi}\Bigg]\Bigg[\sum_j l_j(r)\bar{G}_{sj}\Bigg]\Bigg]d\Omega\Bigg\} \qquad (6.20)\\
&= -F_c^{-1}\Bigg\{ 2\int_{\Omega_k}\Bigg[\frac{\partial\sigma_k}{\partial(\sigma_{\alpha\beta})_k}\vec{\nabla}\bar{G}_p(r)\cdot\vec{\nabla}\bar{G}_s(r) + k_y^2\frac{\partial\sigma_{yy}}{\partial(\sigma_{\alpha\beta})_k}\bar{G}_s\bar{G}_p\Bigg]d\Omega\Bigg\}
\end{aligned}
$$

$$
\begin{aligned}
\frac{\partial G_s(r_p)}{\partial(\sigma_{\alpha\beta})_k} &= -\int_{\Omega_k}\frac{\vec{\partial}\sigma_k}{\vec{\partial}(\sigma_{\alpha\beta})_k}\cdot\vec{\nabla}\Bigg[\sum_i l_i(r)G_{pi}\Bigg]\cdot\vec{\nabla}\Bigg[\sum_j l_j(r)G_{sj}\Bigg]d\Omega \\
&\qquad\qquad (6.21)\\
&= -\int_{\Omega_k}\frac{\vec{\partial}\sigma_k}{\vec{\partial}(\sigma_{\alpha\beta})_k}\cdot\vec{\nabla}G_p(r)\cdot\vec{\nabla}G_s d\Omega
\end{aligned}
$$

Applying the constant point: $\delta\boldsymbol{\sigma}(r)=\delta\boldsymbol{\sigma}_k\delta(r-r_k)$, $r\in\Omega_k$, or constant block: $\delta\boldsymbol{\sigma}(r)=\delta\boldsymbol{\sigma}_k$, $r\in\Omega_k$, model parameterisation schemes to the above equations, one finds that they give the same results as shown by equations (6.11) - (6.14). It means that the perturbation method and the numerical method are equivalent, although the former is derived by application of the self-adjoint differential operator to the perturbation analysis and the latter is based on the linear equation of the model discretization. Both are applicable for DC resistivity anisotropic inversion.

6.5 Sensitivities in Terms of Principal Conductivities and Directions

Instead of working with the components of the conductivity tensor in the geographic frame, we will now consider the derivatives with respect to the principal values (and orientation angles of the symmetry axis) in the natural rock frame, which are the physically meaningful quantities. Let the model parameters be represented by $m_v=(\sigma_1,\sigma_2,\sigma_3,\theta_0,\varphi_0)$

Accordingly, the perturbation of the conductivity tensor may be expressed by $\delta\boldsymbol{\sigma} = \left(\partial\boldsymbol{\sigma}/\partial m_v\right)\delta m_v$ and equations (6.9) and (6.10) become

$$\delta\bar{G}_s\left(r_p\right) = -2\int_{\Omega}\left[\left[\frac{\partial\boldsymbol{\sigma}}{\partial m_v}\vec{\nabla}\bar{G}_s\left(r\right)\right]\cdot\vec{\nabla}\bar{G}_p\left(r\right) + k_y^2\frac{\partial\sigma_{yy}}{\partial m_v}\bar{G}_s\left(r\right)\bar{G}_p\left(r\right)\right]\delta m_v d\Omega \quad (6.22)$$

and

$$\delta G_s\left(r_p\right) = -2\int_{\Omega}\left[\left[\frac{\partial\boldsymbol{\sigma}}{\partial m_v}\vec{\nabla}G_s\left(r\right)\right]\cdot\vec{\nabla}G_p\left(r\right)\right]\delta m_v d\Omega \quad (6.23)$$

Applying a discretisation scheme: constant-point: $\delta m_v\left(r\right) = \delta m_v\delta\left(r - r_k\right)$ $r\in\Omega_k$, or constant block: $\delta m_v\left(r\right) = \delta m_v$ $r\in\Omega_k$, where Ω_k are small sub-domains composing Ω, we have for the Fréchet derivatives:

Constant Point Approximation

2.5-D Case:

$$\frac{\partial G_s\left(r_p\right)}{\partial m_v} = -F_c^{-1}\left\{\left[\frac{\partial\boldsymbol{\sigma}}{\partial m_v}\nabla\bar{G}_s\left(r\right)\right]\cdot\vec{\nabla}\bar{G}_p\left(r\right) + k_y^2\frac{\partial\sigma_{yy}}{\partial m_v}\bar{G}_s\left(r\right)\bar{G}_p\left(r\right)\right\}$$

$$m_v \in \left(\sigma_{x'x'}, \sigma_{y'y'}, \sigma_{z'z'}, \theta_0\right) \quad (6.24)$$

3-D Case:

$$\frac{\partial G_s\left(r_p\right)}{\partial m_v} = -\left[\frac{\partial\boldsymbol{\sigma}}{\partial m_v}\nabla G_s\left(r\right)\right]\cdot\vec{\nabla}G_p\left(r\right)$$

$$m_v \in \left(\sigma_{x'x'}, \sigma_{y'y'}, \sigma_{z'z'}, \theta_0\right) \quad (6.25)$$

Constant Block Approximation

2.5-D Case:

$$\frac{\partial G_s\left(r_p\right)}{\partial m_v} = -w_\alpha F_c^{-1}\left\{\left[\frac{\partial\boldsymbol{\sigma}}{\partial m_v}\vec{\nabla}\bar{G}_s\left(r\right)\right]\cdot\nabla\bar{G}_p\left(r\right) + k_y^2\frac{\partial\sigma_{yy}}{\partial m_v}\bar{G}_s\left(r\right)\bar{G}_p\left(r\right)\right\}\Big|_\alpha$$

$$m_v \in \left(\sigma_{x'x'}, \sigma_{y'y'}, \sigma_{z'z'}, \theta_0\right) \quad (6.26)$$

3-D Case:

$$\frac{\partial G_s\left(r_p\right)}{\partial m_v} = -w_\alpha \left[\frac{\partial \boldsymbol{\sigma}}{\partial m_v} \vec{\nabla} G_s\left(r\right)\right] \cdot \nabla G_p\left(r\right)\Bigg|_\alpha \tag{6.27}$$

$$m_v \in \left(\sigma_{x'x'}, \sigma_{y'y'}, \sigma_{z'z'}, \theta_0\right)$$

Here $\partial\sigma/\partial m_v$ can be calculated by equation (3.13) or (3.14) and w_α are the Gaussian weights. The Cartesian tensor form of equation (6.25), for example, is:

$$\frac{\partial G_s\left(r_p\right)}{\partial\left(m_v\right)} = -\left\{\left(\frac{\partial \sigma_{ij}}{\partial m_v}\frac{\partial G_s}{\partial x_j}\frac{\partial G_p}{\partial x_i}\right)\right\} \tag{6.28}$$

where summation is implied in the above equation through the repetition of subscripts $i, j = x, y, z$ *and* $x_i, x_j = x, y, z$. Expanding out in terms of the various components, the Fréchet derivatives in terms of the principal values may be written as follows for the 3-D case:

$$\begin{aligned}
\frac{\partial G_s}{\partial m_v} = -\Bigg\{ &\frac{\partial \sigma_{xx}}{\partial m_v}\frac{\partial G_s}{\partial x}\frac{\partial G_p}{\partial x} + \frac{\partial \sigma_{yy}}{\partial m_v}\frac{\partial G_s}{\partial y}\frac{\partial G_p}{\partial y} + \frac{\partial \sigma_{zz}}{\partial m_v}\frac{\partial G_s}{\partial z}\frac{\partial G_p}{\partial z} \\
&+ \frac{\partial \sigma_{xy}}{\partial m_v}\left(\frac{\partial G_s}{\partial x}\frac{\partial G_p}{\partial y} + \frac{\partial G_s}{\partial y}\frac{\partial G_p}{\partial x}\right) \\
&+ \frac{\partial \sigma_{xz}}{\partial m_v}\left(\frac{\partial G_s}{\partial x}\frac{\partial G_p}{\partial z} + \frac{\partial G_s}{\partial z}\frac{\partial G_p}{\partial x}\right) \\
&+ \frac{\partial \sigma_{yz}}{\partial m_v}\left(\frac{\partial G_s}{\partial y}\frac{\partial G_p}{\partial z} + \frac{\partial G_s}{\partial z}\frac{\partial G_p}{\partial y}\right)\Bigg\}
\end{aligned} \tag{6.29}$$

where m_v assumes any of the values $\sigma_{x'x'}, \sigma_{y'y'}, \sigma_{z'z'}, \theta_0, \varphi_0$. The sensitivity functions can therefore be computed from knowledge of the Green's functions for the true source G_s (current electrode S) and the adjoint source G_p (potential electrode P), which are obtained as part of the forward modelling (chapter 4) and the partial derivatives of the conductivity tensor with respect to each of the model parameters. The latter can be obtained by differentiating each of the elements of equation (3.13). They are simple trigonometric functions.

In the 2.5-D case $\sigma_{xy} = \sigma_{yz} = 0$ and all derivatives of these quantities go to zero. Also $\sigma_{yy} = \sigma_2$ and so $\dfrac{\partial \sigma_{yy}}{\partial \sigma_2} = 1$ and all other derivatives of σ_{yy} are zero. The remaining non-zero derivatives to consider are:

$$\frac{\partial \sigma_{xx}}{\partial \sigma_1} = \cos^2 \theta_0, \qquad \frac{\partial \sigma_{xx}}{\partial \sigma_3} = \sin^2 \theta_0, \qquad \frac{\partial \sigma_{xx}}{\partial \theta_0} = (\sigma_3 - \sigma_1)\sin 2\theta_0$$

$$\frac{\partial \sigma_{xx}}{\partial \sigma_1} = \sin^2 \theta_0, \qquad \frac{\partial \sigma_{xx}}{\partial \sigma_3} = \cos^2 \theta_0, \qquad \frac{\partial \sigma_{xx}}{\partial \theta_0} = (\sigma_1 - \sigma_3)\sin 2\theta_0 \qquad (6.30)$$

$$\frac{\partial \sigma_{xx}}{\partial \sigma_1} = -\sin \theta_0 \cos \theta_0, \quad \frac{\partial \sigma_{xx}}{\partial \sigma_3} = \sin \theta_0 \cos \theta_0, \quad \frac{\partial \sigma_{xx}}{\partial \theta_0} = 2(\sigma_3 - \sigma_1)\cos 2\theta_0$$

6.5.1 Isotropic Case

In the case of an isotropic medium we have:

$$\sigma_{xx} = \sigma_{yy} = \sigma_{zz} = \sigma \text{ and } \sigma_{xy} = \sigma_{xz} = \sigma_{yz} = 0 \qquad (6.31)$$

every cross term disappears in equation (6.8) and the derivatives $\dfrac{\partial \sigma_{ii}}{\partial m_v}$ are all equal to 1 and equation (6.12) reduces to the dot product of the gradients of the two Green's functions:

$$\frac{\partial G}{\partial \boldsymbol{\sigma}} = -\vec{\nabla} G_s \cdot \vec{\nabla} G_p \qquad (6.32)$$

This is the same result as that obtained by Zhou and Greenhalgh (1999, page 449), using an isotropic formulation

6.5.2 Uniform Anisotropic Earth

The Green's functions in the case of a uniform anisotropic medium can be calculated analytically. In section 3.4, I derived expressions for the potential at some arbitrary position in a uniform TI medium, due to a current source on the surface. In this case, the Green's functions are simply evaluated as the potential divided by the current strength. In the case of the adjoint source (receiver position) we place a current source of strength I at this position

and calculate the potential at the subsurface point in question. Obviously the co-ordinates specified for the true source to point P in the medium will be different to those for the adjoint source, but the functional form is identical.

Using the expression $G = \dfrac{K}{R(1 + (\lambda^2 - 1)\cos^2 \psi)^{1/2}}$ with $K = \dfrac{\lambda \rho_l}{2\pi}$ $\qquad$ (6.33)

we can calculate the derivatives needed using the chain rule as follows :

$$\frac{\partial G}{\partial x} = \frac{\partial G}{\partial \cos \psi}.\frac{\partial \cos \psi}{\partial x} + \frac{\partial G}{\partial R}.\frac{\partial R}{\partial x},$$
$$\frac{\partial G}{\partial y} = \frac{\partial G}{\partial \cos \psi}.\frac{\partial \cos \psi}{\partial y} + \frac{\partial G}{\partial R}.\frac{\partial R}{\partial y},$$
$$\frac{\partial G}{\partial z} = \frac{\partial G}{\partial \cos \psi}.\frac{\partial \cos \psi}{\partial z} + \frac{\partial G}{\partial R}.\frac{\partial R}{\partial z}$$
$\qquad$ (6.34)

The various terms appearing in equation (6.34) can be evaluated thus:

$$\frac{\partial G}{\partial \cos \psi} = \frac{-K\left(\lambda^2 - 1\right)\cos \psi}{R\left(1 + \left(\lambda^2 - 1\right)\cos^2 \psi\right)^{3/2}}$$
$\qquad$ (6.35)

$$\frac{\partial G}{\partial R} = \frac{-K}{R^2\left(1 + \left(\lambda^2 - 1\right)\cos^2 \psi\right)^{1/2}}$$
$\qquad$ (6.36)

$$\frac{\partial R}{\partial x} = \frac{x}{R}, \qquad \frac{\partial R}{\partial y} = \frac{y}{R}, \qquad \frac{\partial R}{\partial z} = \frac{z}{R}$$
$\qquad$ (6.37)

The other derivatives of $\cos \psi$ with respect to x, y and z must also be obtained implicitly because of the x, y, and z dependence in the ϕ $\;$ and $\;$ θ terms which make up $\cos \psi$, viz. equation (3.25).

They are:

$$\frac{\partial \cos \psi}{\partial x} = \frac{\partial \cos \psi}{\partial \phi} \cdot \frac{\partial \phi}{\partial x} + \frac{\partial \cos \psi}{\partial \theta} \cdot \frac{\partial \theta}{\partial x}$$

$$\frac{\partial \cos \psi}{\partial y} = \frac{\partial \cos \psi}{\partial \phi} \cdot \frac{\partial \phi}{\partial y} + \frac{\partial \cos \psi}{\partial \theta} \cdot \frac{\partial \theta}{\partial y} \qquad (6.38)$$

$$\frac{\partial \cos \psi}{\partial z} = \frac{\partial \cos \psi}{\partial \phi} \cdot \frac{\partial \phi}{\partial z} + \frac{\partial \cos \psi}{\partial \theta} \cdot \frac{\partial \theta}{\partial z}$$

where

$$\frac{\partial \cos \psi}{\partial \phi} = -\sin \theta_0 \sin \theta \sin(\phi - \phi_0) = -\sin \theta_0 \sin \theta (\sin \phi \cos \phi_0 - \cos \phi \sin \phi_0)$$

$$\frac{\partial \cos \psi}{\partial \theta} = \sin \theta_0 \cos(\phi - \phi_0) \cos \theta - \cos \theta_0 \sin \theta \qquad (6.39)$$

The other derivatives for $\partial \theta / \partial x, \partial \theta / \partial y, \partial \theta / \partial z, \partial \phi / \partial x, \partial \phi / \partial y, \partial \phi / \partial z$ appearing in equation (6.38) are derived in appendix B, and shown to be:

$$\frac{\partial \theta}{\partial x} = \frac{xz}{R^2 .(x^2 + y^2)^{1/2}}$$

$$\frac{\partial \theta}{\partial y} = \frac{yz}{R^2 .(x^2 + y^2)^{1/2}} \qquad (6.40)$$

$$\frac{\partial \theta}{\partial z} = \frac{(x^2 + y^2)^{1/2}}{R^2}$$

and

$$\frac{\partial \phi}{\partial z} = 0$$

$$\frac{\partial \phi}{\partial x} = -\frac{y}{x^2 + y^2}$$

$$\frac{\partial \phi}{\partial y} = \frac{1}{x.(1 + y^2 / x^2)} \qquad (6.41)$$

In the case of an isotropic medium $\lambda = 1$ and equation (6.35) is equal to zero. This yields all of the first set of terms on the right hand side of equation (6.34) equal to zero, and therefore no dependence of the Fréchet derivatives on the polar angles ϕ_0, θ_0. Equation (6.36) takes on the much simpler form $- K / R^2$, independent of $\cos \psi$.

Returning to the anisotropic case, we have shown above that all of the required spatial derivatives of the Green's functions can be computed in terms of the elementary functions involving the position co-ordinates x,y,z for the subsurface point in question, be it measured from either the real current source or the adjoint current source.

It remains to calculate the various derivatives of the conductivity tensor with respect to the chosen parameters. In the TTI case this involves the following terms:

$$\frac{\partial \sigma_{xx}}{\partial \sigma_l}, \quad \frac{\partial \sigma_{xx}}{\partial \sigma_t}, \quad \frac{\partial \sigma_{xx}}{\partial \theta_0}, \quad \frac{\partial \sigma_{xx}}{\partial \phi_0}$$

$$\frac{\partial \sigma_{yy}}{\partial \sigma_l}, \quad \frac{\partial \sigma_{yy}}{\partial \sigma_t}, \quad \frac{\partial \sigma_{yy}}{\partial \theta_0}, \quad \frac{\partial \sigma_{yy}}{\partial \phi_0}$$

$$\frac{\partial \sigma_{zz}}{\partial \sigma_l}, \quad \frac{\partial \sigma_{zz}}{\partial \sigma_t}, \quad \frac{\partial \sigma_{zz}}{\partial \theta_0}, \quad \frac{\partial \sigma_{zz}}{\partial \phi_0}$$

$$\frac{\partial \sigma_{xy}}{\partial \sigma_l}, \quad \frac{\partial \sigma_{xy}}{\partial \sigma_t}, \quad \frac{\partial \sigma_{xy}}{\partial \theta_0}, \quad \frac{\partial \sigma_{xy}}{\partial \phi_0}$$

$$\frac{\partial \sigma_{xz}}{\partial \sigma_l}, \quad \frac{\partial \sigma_{xz}}{\partial \sigma_t}, \quad \frac{\partial \sigma_{xz}}{\partial \theta_0}, \quad \frac{\partial \sigma_{xz}}{\partial \phi_0}$$

$$\frac{\partial \sigma_{yz}}{\partial \sigma_l}, \quad \frac{\partial \sigma_{yz}}{\partial \sigma_t}, \quad \frac{\sigma_{yz}}{\partial \theta_0}, \quad \frac{\partial \sigma_{yz}}{\partial \phi_0}$$

These derivatives can be easily calculated from equations (3.16) and (3.17).

6.5.3 The 2.5-D Case – Profile Perpendicular to Strike

We will now look at the special 2.5-D case in which the profile is assumed to be perpendicular to strike. Therefore the effect of azimuth can be ignored. In this situation we have $\sigma_{xy} = \sigma_{yz} = 0$ and all derivatives involving these components go to zero.

Referring to equation (6.30) and putting $\sigma_1 = \sigma_2 = \sigma_l$, and $\sigma_3 = \sigma_t$, the only tensor derivative components to consider are:

$$\frac{\partial \sigma_{xx}}{\partial \sigma_l} = \cos^2 \theta_0, \quad \frac{\partial \sigma_{xx}}{\partial \sigma_t} = \sin^2 \theta_0, \quad \frac{\partial \sigma_{xx}}{\partial \theta_0} = (-\sigma_l + \sigma_t) \sin 2\theta_0, \quad \frac{\partial \sigma_{xx}}{\partial \phi_0} = 0$$

$$\frac{\partial \sigma_{yy}}{\partial \sigma_l} = 1, \quad \frac{\partial \sigma_{yy}}{\partial \sigma_t} = \frac{\partial \sigma_{yy}}{\partial \theta_0} = \frac{\partial \sigma_{yy}}{\partial \phi_0} = 0$$

$$\frac{\partial \sigma_{xz}}{\partial \sigma_l} = \frac{-\partial \sigma_{xz}}{\partial \sigma_t} = 0.5 \sin 2\theta_0, \quad \frac{\partial \sigma_{xz}}{\partial \theta_0} = (-\sigma_l + \sigma_t) \cos 2\theta_0, \quad \frac{\partial \sigma_{xz}}{\partial \phi_0} = 0$$

$$\frac{\partial \sigma_{zz}}{\partial \sigma_l} = \sin^2 \theta_0, \quad \frac{\partial \sigma_{zz}}{\partial \sigma_t} = \cos^2 \theta_0, \quad \frac{\partial \sigma_{zz}}{\partial \theta_0} = (\sigma_l - \sigma_t) \sin 2\theta_0, \quad \frac{\partial \sigma_{zz}}{\partial \phi_0} = 0$$

(6.31)

Substituting into equation (6.29), replacing the source subscript s by the superscript A (for current electrode) and the adjoint source subscript p by the superscript M (for potential electrode) we obtain the following expressions for the sensitivities:

$$\frac{\partial U}{\partial \sigma_l} = -\left\{ \cos^2 \theta_0 \frac{\partial G^A}{\partial x} \frac{\partial G^M}{\partial x} + \frac{\partial G^A}{\partial y} \frac{\partial G^M}{\partial y} + \sin^2 \theta_0 \frac{\partial G^A}{\partial z} \frac{\partial G^M}{\partial z} \right.$$
$$\left. + 0.5 \sin 2\theta_0 \left(\frac{\partial G^A}{\partial x} \frac{\partial G^M}{\partial z} + \frac{\partial G^A}{\partial z} \frac{\partial G^M}{\partial x} \right) \right\}$$

$$\frac{\partial U}{\partial \sigma_t} = -\sin^2 \theta_0 \frac{\partial G^A}{\partial x} \frac{\partial G^M}{\partial x} - \cos^2 \theta_0 \frac{\partial G^A}{\partial z} \frac{\partial G^M}{\partial z}$$
$$+ 0.5 \sin 2\theta_0 \left(\frac{\partial G^A}{\partial x} \frac{\partial G^M}{\partial z} + \frac{\partial G^A}{\partial z} \frac{\partial G^M}{\partial x} \right)$$

(6.32)

$$\frac{\partial U}{\partial \theta_0} = -(\sigma_l + \sigma_t) \sin 2\theta_0 \frac{\partial G^A}{\partial x} \frac{\partial G^M}{\partial x} - (\sigma_l + \sigma_t) \sin 2\theta_0 \frac{\partial G^A}{\partial z} \frac{\partial G^M}{\partial z}$$
$$- (\sigma_l + \sigma_t) \cos 2\theta_0 \left(\frac{\partial G^A}{\partial x} \frac{\partial G^M}{\partial z} + \frac{\partial G^A}{\partial z} \frac{\partial G^M}{\partial x} \right)$$

In the isotropic case $(\sigma_l = \sigma_t = \sigma)$ we find that $\partial U / \partial \theta_0 = 0$ and the Fréchet derivative

$$\frac{\partial U}{\partial \sigma} = \frac{1}{2}(\frac{\partial U}{\partial \sigma_l} + \frac{\partial U}{\partial \sigma_t})$$ leads to a cancellation of all cross terms involving the Green's

functions and elimination of all θ_0 dependence, yielding the same result as equation (6.32).

Note that $\partial U / \partial \rho = -\frac{1}{\rho^2} \partial U / \partial \sigma$, yielding a change of sign between the conductivity and

resistivity sensitivities.

6.6 Illustrative Examples

To illustrate the nature of the Fréchet derivatives, we first consider the simple case of a 3-D homogeneous, isotropic earth. The current electrode is located at (5,0,0) and the potential electrode at (10,0,0). The ground conductivity is 0.1 S/m (resistivity 10 Ω-m). Figure 6.2 shows the Fréchet derivatives at two depth slices Z = 0 and Z = 0.5 units, as well as in cross section form for a profile through both electrodes. Note the symmetry of the patterns and the decrease of sensitivity with depth.
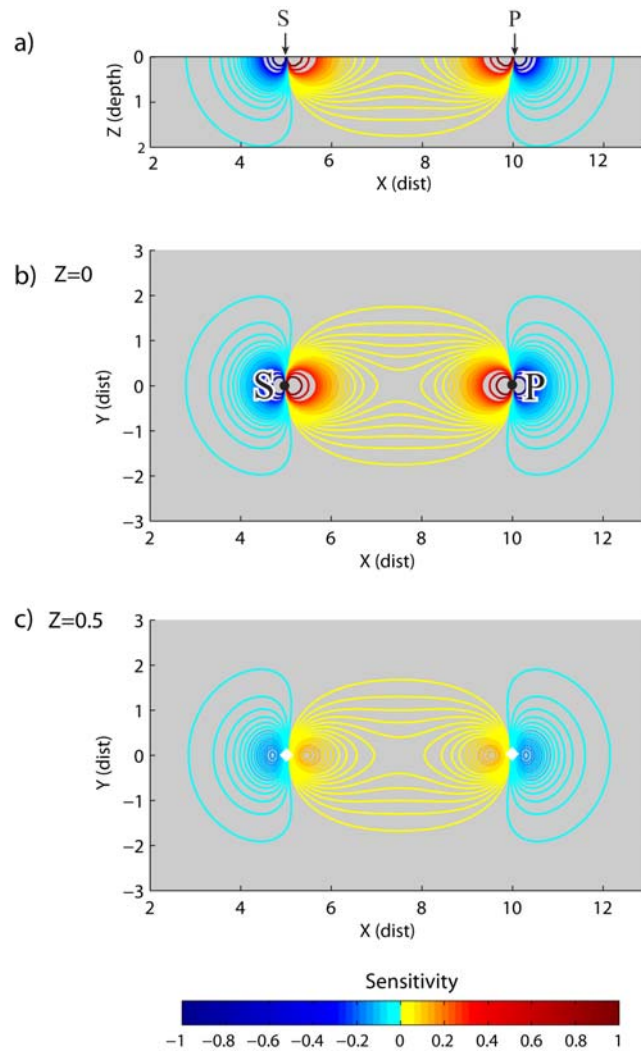
Figure 6.2. Fréchet derivative *dG/dσ* for an isotropic model having conductivity 0.1 S/m. The current source is at (5,0,0) and the potential electrode at (10,0,0). Both cross-sectional view at Y = 0 (diagram a) and two horizontal depth slices at Z = 0 and Z = 0.5 (diagrams b and c) depicting sensitivity variations in plan view are shown. For the Z = 0.5 depth slice, the electrode positions, shown by white diamonds, have been projected onto this plane.

The sensitivities are largest in magnitude in the vicinity of the electrodes. The derivatives actually change sign around the electrodes, being positive between the electrodes and negative either side. An increase in conductivity in a region of positive sensitivity results in a greater potential being measured, whereas a decrease in conductivity in a positive sensitivity region decreases the measured potential value. The opposite applies for the negative sensitivity regions.

Next we consider a homogeneous, anisotropic model having a tilted axis of symmetry. The longitudinal conductivity (0.1 S/m) is four times larger than the transverse conductivity (0.025 S/m), yielding a coefficient of anisotropy λ of 2. Again the current electrode is located at (5,0,0) and the potential electrode at (10,0,0). In the first set of plots the strike of the plane of stratification is held fixed at 90° ($\varphi_0 = 0°$). The dip angle θ_0 (measured from the horizontal,

left of source in constrast to chapter 5 images) is allowed to vary from 0 (horizontal beds) to 90° (vertical plane of stratification).

Figure 6.3 shows a series of cross sections in the X-Z plane (Y = 0) for the longitudinal conductivity Fréchet derivative $dG/d\sigma_l$. Each plot corresponds to a different dip – 0, 15, 45, 75 and 90°. The sensitivity pattern for $\theta_0 = 0°$ is very similar to the isotropic equivalent; the contours are concentrated towards the surface and elongated along it. This is confirmed in the plan view display (figure 6.4) which shows the sensitivity values at the surface as a function of position. The positive contours are stretched along the line intersecting the electrodes (x axis). Also it can be seen in Figure 6.4 that the negative sensitivity contour sections are extended greatly along the strike direction (y axis) and show some curvature towards the opposite electrode, as a departure from the isotropic pattern.

The sensitivity patterns in the X-Z plane (figure 6.3) for all dips other than 0° are distinctly asymmetrical, with the contours elongated in the plane of stratification. Sensitivity is thus smallest in magnitude along lines orthogonal to the stratification. All plots exhibit shifts of both the negative and positive contours of sensitivity such that they follow the direction of highest conductivity (orthogonal to $\hat{z}'$). The surface display (figure 6.4) shows that the sensitivity decreases markedly with increasing θ_0. For all angles the surface sensitivity pattern is symmetrical about the line intersecting the electrodes. For the vertically dipping beds the sensitivity values are very low in magnitude and entirely negative.
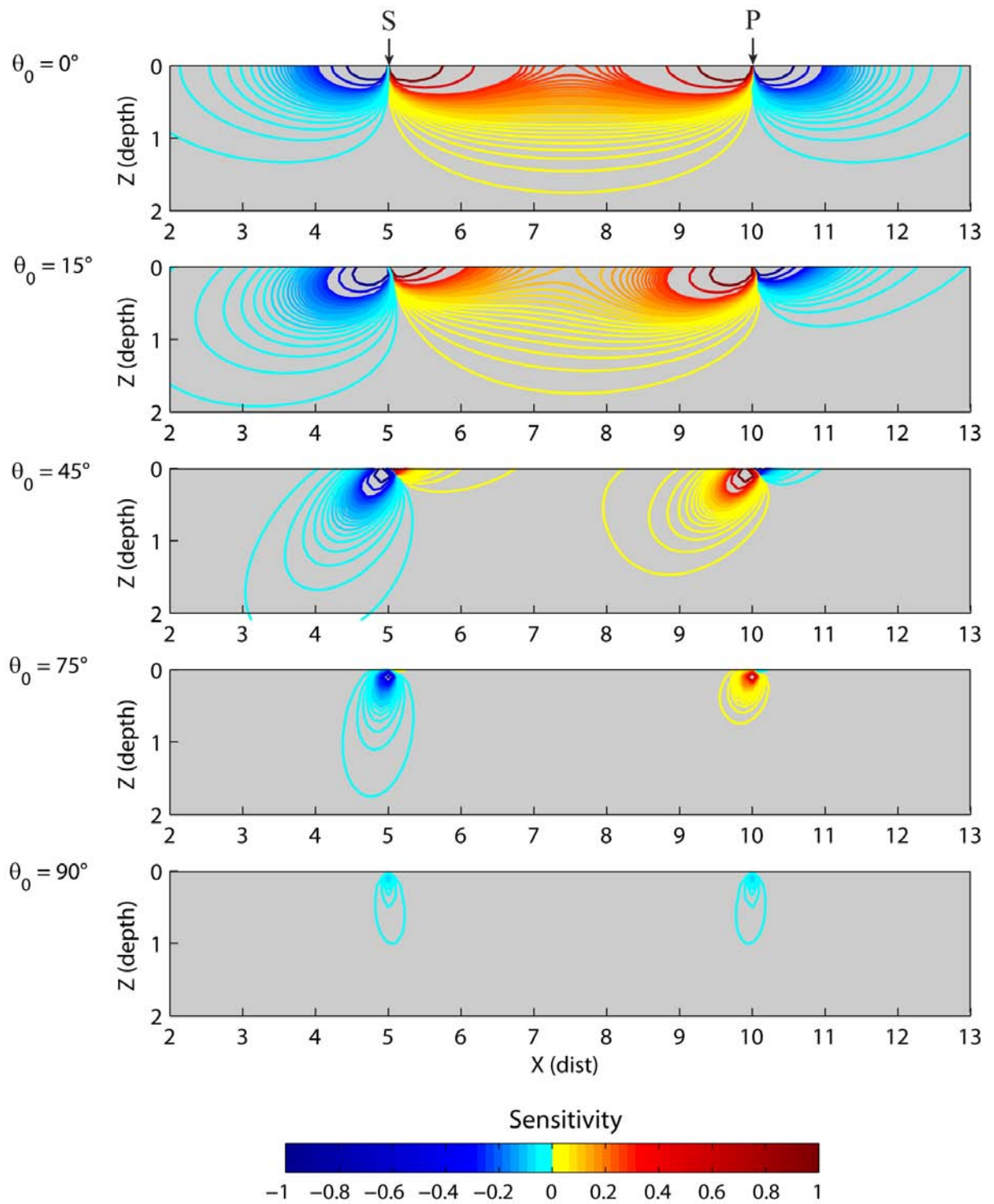
Figure 6.3.   Longitudinal conductivity Fréchet derivative $dG/d\sigma_l$ variations in the subsurface for an anisotropic model, having longitudinal conductivity 0.1 S/m, transverse conductivity 0.025 S/m, and strike of the symmetry axis of 0º.   The various sensitivity plots shown are for different dips of the symmetry axis, $\theta_0 = 0, 15, 45, 75, 90$ degrees. The profiles are perpendicular to strike of the plane of stratification.   The electrodes are again at (5,0,0) and (10,0,0).
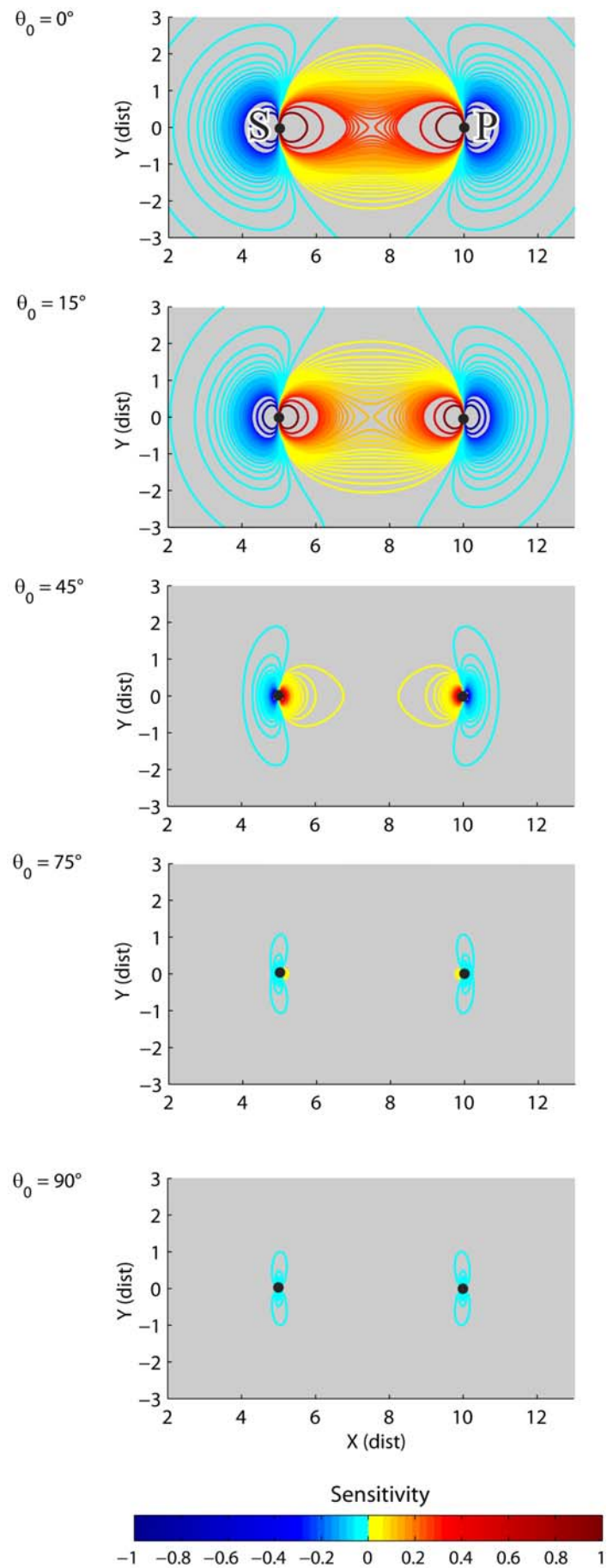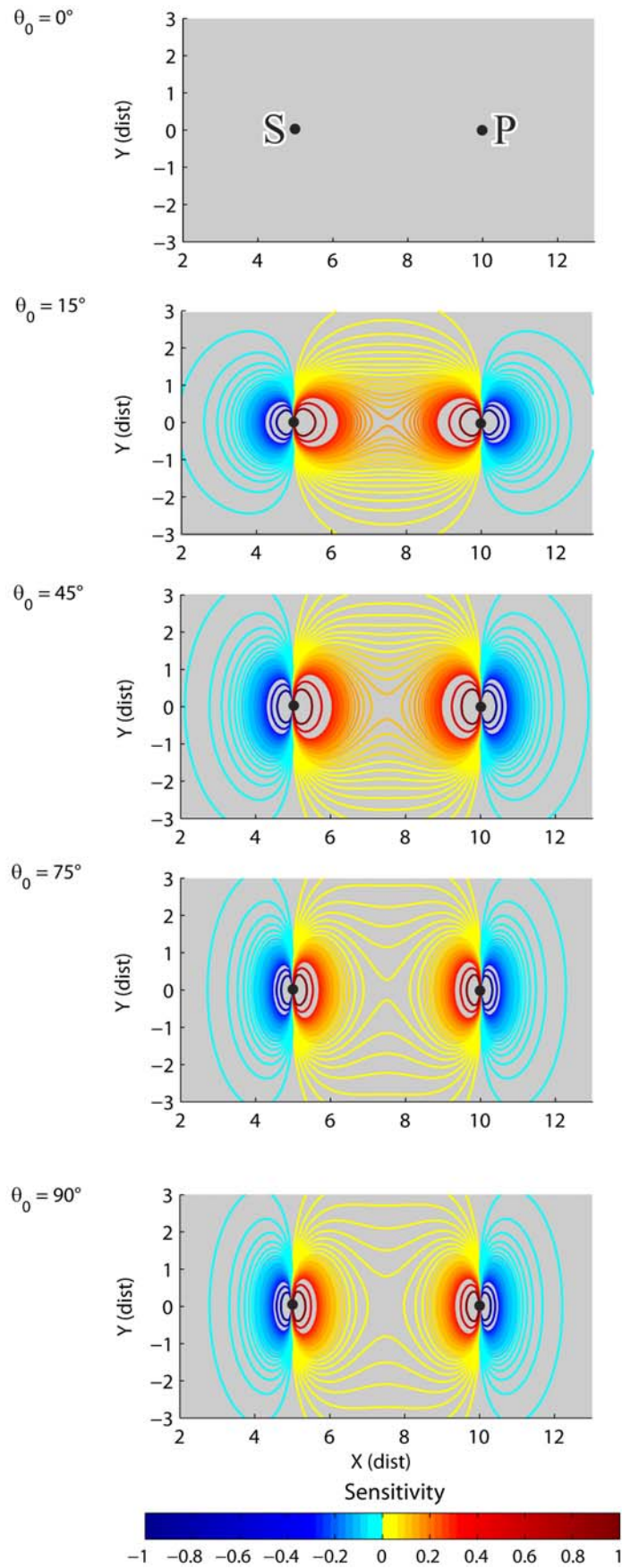
Figure 6.4. Fréchet derivative $dG/d\sigma_l$ plots at the surface (Z=0) for the same model and electrode configuration as figure 6.3. Note the symmetry of the plots and the decrease in sensitivity with increasing dip.

The corresponding plots for the transverse resistivity Fréchet derivatives $dG/d\sigma_t$ are given in figure 6.5 and figure 6.6. For a vertical axis of symmetry ($\theta_0 = 0°$) the sensitivities are entirely negative, with two regions of large negative sensitivity beneath the electrodes. The two regions are elongated towards each other. The Z = 0 depth slice (figure 6.6) shows no sensitivity at the surface. For dips of 15, 45 and 75 degrees, the sensitivity patterns in the X-Z plane are all asymmetrical (figure 6.5), the contours being elongated in a direction parallel to the dip of stratification. The steepness of the pattern increases with increasing θ_0. In comparison with the corresponding $dG/d\sigma_l$ patterns (figure 6.3) there is greater sensitivity at depth. Although the contours are elongated in a direction parallel to the stratification, sensitivity is smallest in magnitude along the lines drawn through separate electrodes and parallel to the stratification. This is in marked contrast to $dG/d\sigma_l$, which exhibits greatest sensitivity in this direction. For the surface (Z=0) slices (figure 6.6), the patterns are all symmetric about the X axis, and elongated in the strike direction. The transverse conductivity sensitivity for a dip of 90° shows a symmetric pattern that resembles the isotropic plot elongated in the vertical direction (along the plane of stratification).

Finally, we show the effect of azimuth of the symmetry axis on the sensitivity patterns. Figures 6.7, 6.8 and 6.9 are plots of $dG/d\sigma_t$ for the same anisotropic structure and electrode configuration, but this time for a strike of the symmetry axis of 45° (plane of stratification strike = 45 + 90 = 135°). From the surface slices (Z = 0) shown in figure 6.8, it can be seen that the x axis symmetry is broken as a result of the bedding plane strike no longer being 90°. If two imaginary lines are drawn through the electrodes in the strike direction ($\varphi_0 + 90°$), the regions of positive and negative sensitivities do not cross boundaries defined by these lines and are largest in value orthogonal to the strike and close to the electrodes. The cross-section displays for the X-Z plane (figure 6.7) show a progressive tilting of the sensitivity patterns as dip increases. The $\theta_0 = 0°$ plot is entirely negative and symmetrical. All other dip angles yield both positive and negative sensitivities, and are asymmetrical because the cross-section is not perpendicular to strike. Only at a dip of $\theta_0 = 90°$ is the symmetry restored. Interestingly, the sensitivity is actually zero at all points on the surface for a dip of 0° (figure 6.8), but for other dips the magnitude of the sensitivity is appreciable and the contours extend to modest depths. Figure 6.9 shows the sensitivity variations in plan view at a depth of Z = 0.5 units. There is considerable change in the pattern for dips over the range 0 to 45°, after which the pattern looks very similar. The contours are elongated in the direction of the strike of the stratification plane (maximum conductivity direction).
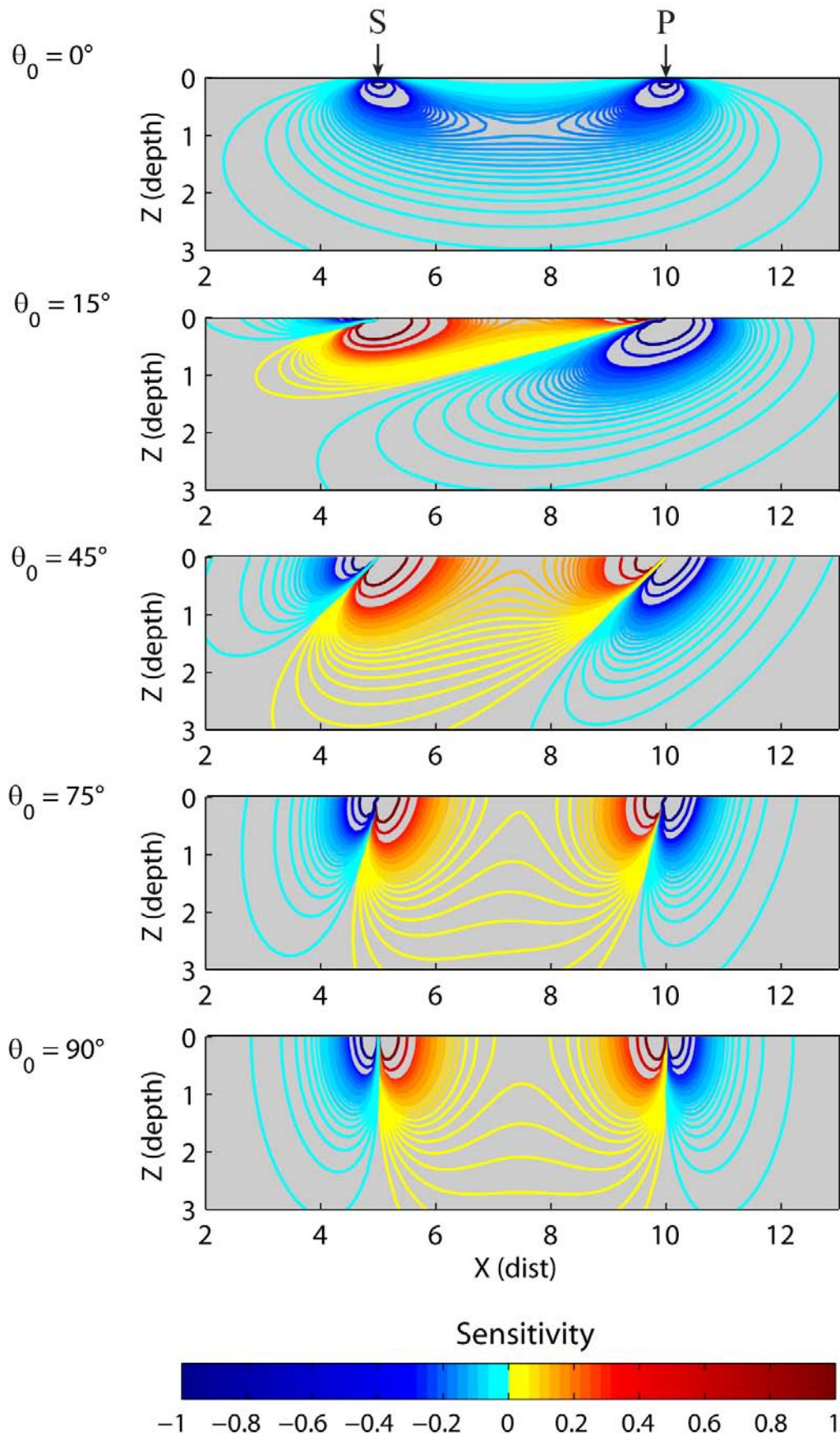
Figure 6.5. Transverse conductivity Fréchet derivative $dG/d\sigma_t$ variations for the same anisotropic model and electrode configuration as in figure 6.3. The various sensitivity plots are for differing dips of the symmetry axis, as indicated. The profiles are perpendicular to the strike of the plane of stratification.

Figure 6.6. Fréchet derivative $dG/d\sigma_t$ plots at the surface (Z=0) for the same model and electrode configuration as in figure.6.5. All patterns are symmetrical about the *x* axis. In the case of zero dip the sensitivity is zero.
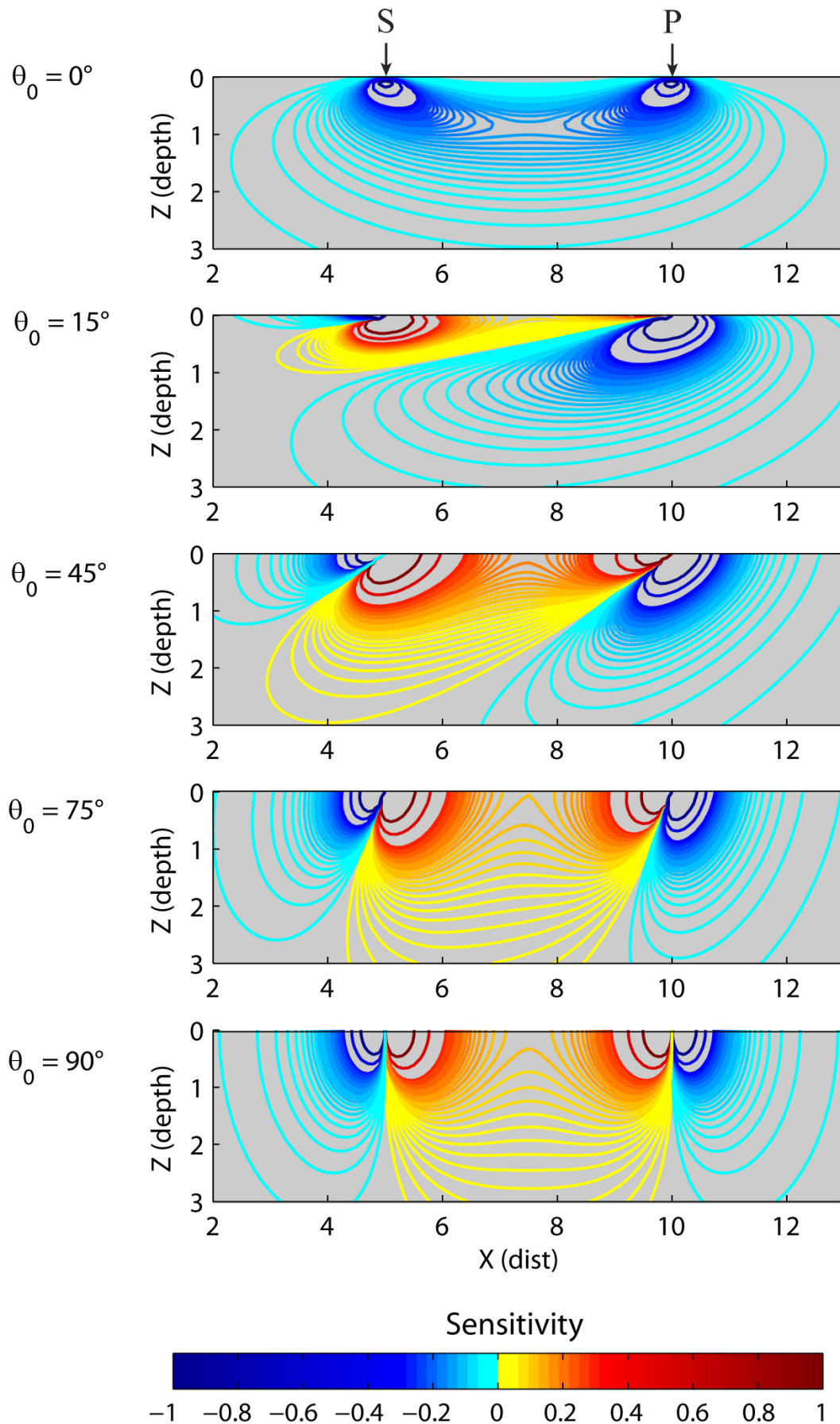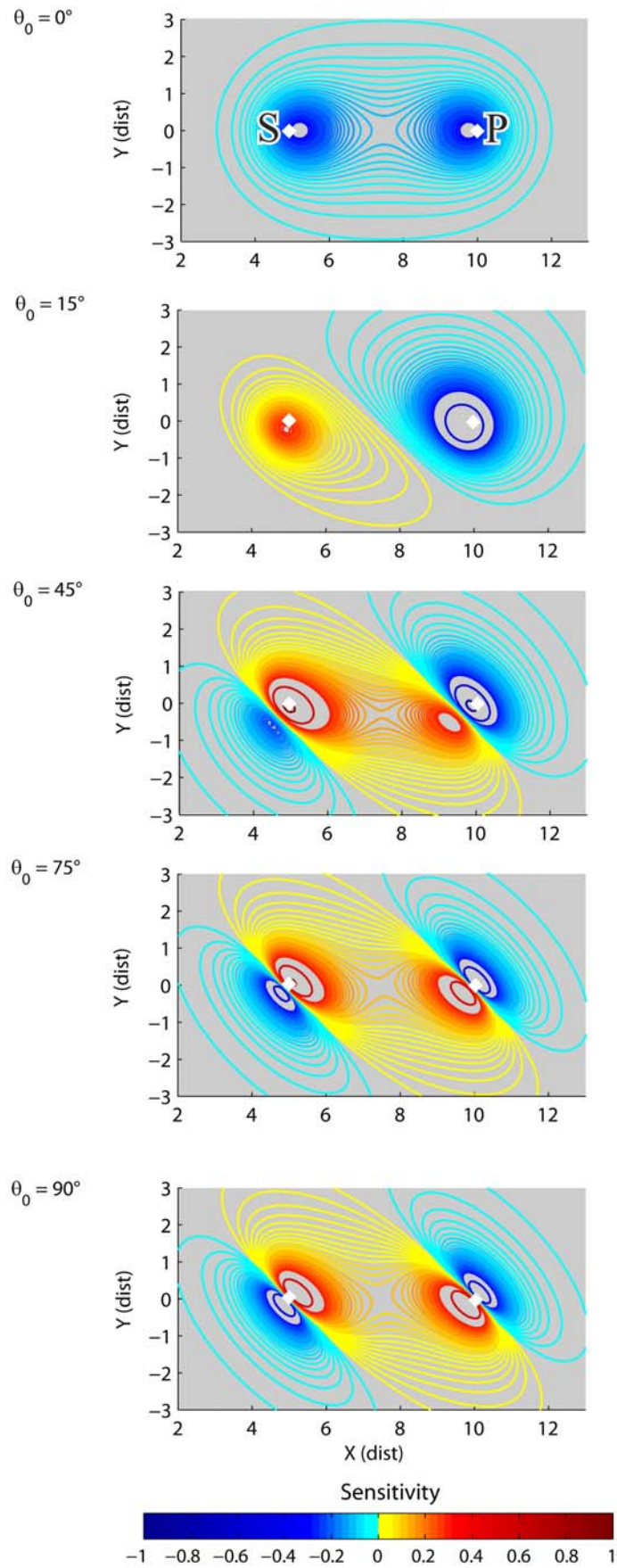
Figure 6.7. Sensitivity variations $dG/d\sigma_t$ for the same model as figure 6.3, but the strike of the symmetry axis is now 45° and not 0°. The dip is again reflected in the asymmetry and steepening of the patterns. The contours are elongated in the direction of plane of stratification.
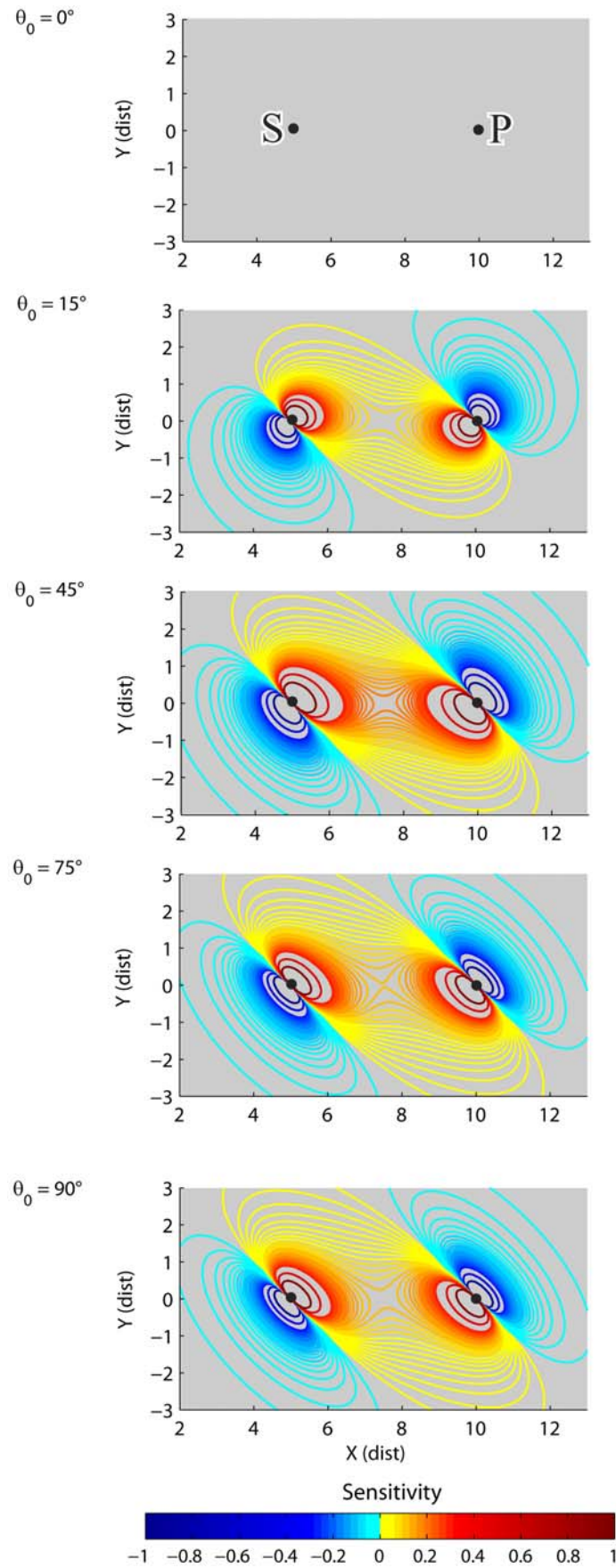
Figure 6.8. Companion surface sensitivity plots for figure 6.7. The 45° strike is now reflected in the asymmetry about the *x* axis and an alignment of the patterns parallel to the strike of the plane of stratification.

Figure 6.9. Depth slices at Z = 0.5 units, showing transverse conductivity sensitivity variations in plan view for the same TTI model having 45° strike, and various dips. Note the sudden changes in the pattern for between dips of 0° and 45°. The projected electrode positions onto the Z = 0.5 plane are shown as white diamonds.

Chapter 7

Conclusions and Future Research

I have presented a new Gaussian quadrature grid scheme for 2.5-D/3-D DC resistivity modelling. The method is particularly suitable for numerical simulation of a complex geological model having the most general anisotropy and an arbitrary topographic surface. The formulation shows that it is close to the spectral element method, but it does not require the constant-element mesh matching a topographic earth surface due to invoking a Gaussian quadrature grid for the sub-domains covering the whole model. Local cardinal functions are used to determine the partial derivatives of the Green's functions at each Gaussian abscissae which appear in the functional to be minimised. Sub-domain integration and summation leads to a system of linear equations to be solved, using standard iterative or matrix inversion techniques. The new method is compared against analytic solutions and finite element solutions for both simple and complex models. The models include homogeneous and inhomogeneous structures with embedded resistive and conductive anomalies. Both isotropic and anisotropic backgrounds are considered, with the surface topography being flat or variable. The new method was found to be highly accurate except in the vicinity of the source (errors still less than 1%) and much easier to deal with anisotropic models having a surface topography than any other traditional numerical method.

Having established a new modelling procedure the next step was to investigate the Fréchet derivatives or sensitivity functions in anisotropic media. The sensitivity functions are required in both experimental design as well as in inversion of resistivity data for updating the model parameters. Previous treatments are based almost exclusively on an isotropic assumption, which is questionable when the ground is anisotropic. In this thesis I present a general perturbation formulation for computing the Fréchet derivatives in 3-D and 2.5-D resistivity inversion, for a model which is both heterogeneous and anisotropic. The formulation involves the Green's functions for the true current source and the adjoint source. These must be computed using a numerical method such as the finite element method or the new Gaussian quadrature grid approach. The equations also involve the derivatives of the conductivity tensor with respect to the principal conductivity values and orientation angles of the symmetry axis. I have derived analytic formulae for computing these derivatives for a very general class of anisotropy, as well as for the special case of a tilted transversely isotropic (TTI) medium.

The thesis also reviews the basic properties of the electric conductivity tensor and the tensor ellipsoid. Equations are developed for computing the six individual components of the tensor in terms of the principal conductivities and the angles defining the major symmetry axis.

The special case of a 3-D homogeneous TTI medium has been studied in considerable detail. I develop analytic solutions for the electric potential, current density and Fréchet derivatives at any interior point within such a medium. The current electrode is assumed to be on the surface of the Earth and the plane of stratification given arbitrary strike and dip. Profiles can be computed for any azimuth. The equipotentials exhibit an elliptical pattern and are not orthogonal to the current density vectors, which are strongly angle dependent. Current density reaches its maximum value in a direction parallel to the longitudinal conductivity direction. Illustrative examples of the Fréchet derivatives are given for the 2.5-D problem, in which the profile is taken perpendicular to strike. All three derivatives of the Green's function with respect to longitudinal conductivity, transverse resistivity and dip angle of the symmetry axis ($dG/d\sigma_l, dG/d\sigma_t, dG/d\theta_0$) show a strongly asymmetric pattern compared to the isotropic case. The patterns are aligned in the direction of the tilt angle.

Examples are presented showing the sensitivity patterns in both plan and cross–sectional view for the homogeneous TTI medium in which the dip and strike of the symmetry axis are varied. These anisotropic sensitivity plots show some general trends previously unreported. The patterns are compared against that for an isotropic medium. For the longitudinal conductivity Fréchet derivative, regions of sensitivity are located along the lines intersecting the electrodes in the direction of the stratification plane. Sensitivity decreases with distance away from this axis (and distance from the electrode). Perpendicular to this axis there is little to no sensitivity. This trend holds for sensitivities both on the surface and at depth, where it is apparent that the contours are elongated along lines perpendicular to the dip. For the transverse resistivity Fréchet derivative there is zero sensitivity along the lines intersecting the respective electrodes that run parallel to the stratification plane. However, the largest sensitivity regions are centred on a line intersecting the respective electrode that runs orthogonal to the stratification. The regions are elongated along the stratification plane, but do not intersect the lines that run parallel from the electrodes. The examples presented also show significant differences in the sensitivities compared to the isotropic pattern. Therefore, failure to account for anisotropy (where it exists) in an inversion could result in false deductions about the subsurface structure.

This thesis has concentrated on theoretical development and testing of new code for numerical resistivity modelling in heterogeneous, anisotropic media, and computation of the Fréchet derivatives. The next step, would be to extensively use the software for a variety of purposes. This can be grouped into four main areas:

1. *Simulations*

- Develop a better understanding of the electrical response of various (simulated) geological structures
- Answer basic questions on detectability and resolution of various targets
- Understand effects of anisotropy on resistivity measurements, and to separate from effects of heterogeneity
- Perform simulations to study resolution of subtle features such as bed thickness, multiple layers, faulting, dyke thickness etc

2. *Sensitivity Analysis*

- Carry out a systematic analysis of the influence of the key anisotropy parameters (longitudinal conductivity, transverse conductivity, coefficient of anisotropy, mean resistivity, dip and azimuth of the axis of symmetry) on the sensitivity functions
- Compare sensitivity functions for different electrode arrays (e.g., Pole-Pole, Wenner, Dipole-Dipole, Square)
- Examine sensitivity for embedded anomalies in an anisotropic background medium and compare with the isotropic case.
- Identify key features which limit performance of ERT (Electrical Resistivity Tomography) e.g., spatial variations in electrical properties of structures, out-of-plane effects, sparse line spacing, inadequate array length

3. *Experimental Design*

- Study the characteristics of the Hessian matrix and the resolution matrix in anisotropic media and compare eigenvalue spectra for different electrode combinations
- Examine the use of grid (areal) electrode arrays as a precursor to full 3-D surveying, in order to improve cross-line correlation and resolution in the 3rd dimension between 2-D lines

- Numerically investigate tensor measurements in 3-D surface arrays, with current and voltage bipoles in various parallel and perpendicular orientations, as a means of detecting anisotropy and better imaging the subsurface

- Assess ability of crosshole 3-D surveying to map complex and steeply dipping structures

4. *Inversion*

- Incorporate the new anisotropic modelling and sensitivity functions into 2.5-D and 3-D resistivity inversion code

- Improve imaging, especially at depth, through combination surface, crosshole, and surface to borehole data inversion, and by incorporation of electrical property data (especially anisotropy) as constraints

- Build mixed precision solver(s) (LU / CG) on the Cell BE architecture for significant speed-up of GQG forward modelling on a field PC.